

## Article

# Ciprofloxacin Uptake from an Aqueous Solution via Adsorption with $K_2CO_3$ -Activated Biochar Derived from Brewing Industry Bagasse

Víctor Francisco Meseguer, Juan Francisco Ortuño , María Isabel Aguilar \* , Mercedes Lloréns , Ana Belén Pérez-Marín  and Emmanuel Fuentes

Departamento de Ingeniería Química, Facultad de Química, Universidad de Murcia, Campus de Espinardo, 30100 Murcia, Spain; vzapata@um.es (V.F.M.); jfortuno@um.es (J.F.O.); llorens@um.es (M.L.); abelenpm@um.es (A.B.P.-M.); tecaguaumu1@um.es (E.F.)

\* Correspondence: maguilar@um.es; Tel.: +34-868887091

**Abstract:** Ciprofloxacin (CPX), an antibiotic considered as an emerging contaminant, needs to be removed from aquatic environments. This work investigates the adsorption of CPX on  $K_2CO_3$ -activated biochar (AB). The biochar was obtained via the pyrolysis of barley bagasse from the brewing industry, and then it was activated with 2M of  $K_2CO_3$ . The activated biochar was characterised using FTIR spectroscopy and a  $pH_{PZC}$  assay. Batch adsorption tests were performed to study the influence of pH and temperature on CPX sorption and to obtain kinetic and equilibrium data. The adsorption of CPX on AB was favoured by increasing the temperature from 10 °C to 55 °C, demonstrating the endothermic nature of the process. The level of CPX removal after 24 h of contact and at pH 3.5 was 82% of that obtained when equilibrium was reached. The kinetic study showed that the adsorption is well described by the Elovich and the Bangham kinetic models. The adsorption is favourable, and the best fits to the experimental equilibrium data were obtained with the Freundlich, Redlich–Peterson and Sips isotherms. In an acidic solution (pH = 3.5) and at 25 °C, the maximum CPX adsorption capacity of AB was  $\approx 105 \text{ mg}\cdot\text{g}^{-1}$ , comparable to that reported for other adsorbents.

**Keywords:** adsorption; activated biochar; adsorption kinetic; bagasse; ciprofloxacin; isotherms



**Citation:** Meseguer, V.F.; Ortuño, J.F.; Aguilar, M.I.; Lloréns, M.; Pérez-Marín, A.B.; Fuentes, E. Ciprofloxacin Uptake from an Aqueous Solution via Adsorption with  $K_2CO_3$ -Activated Biochar Derived from Brewing Industry Bagasse. *Processes* **2024**, *12*, 199. <https://doi.org/10.3390/pr12010199>

Academic Editors: Jan Derco, Andreja Žgajnar Gotvajn and Angelika Kassai

Received: 1 December 2023

Revised: 10 January 2024

Accepted: 15 January 2024

Published: 17 January 2024



**Copyright:** © 2024 by the authors. Licensee MDPI, Basel, Switzerland. This article is an open access article distributed under the terms and conditions of the Creative Commons Attribution (CC BY) license (<https://creativecommons.org/licenses/by/4.0/>).

## 1. Introduction

Until a few years ago (at the end of the 20th century), there was no particular interest in the pollution potential of the presence of pharmaceuticals and personal care products in general, and of antibiotics in particular, in water streams. These compounds are present in the effluents of pharmaceutical manufacturing plants, hospitals, farms and households. Most are persistent and poorly biodegradable. Because they cannot be completely eliminated in conventional wastewater treatment plants, concern about their occurrence and fate in the environment has increased over the last few decades. In addition, antibiotics are designed to act on biological targets, so they can be very harmful to microorganisms and interfere with the proper functioning of wastewater treatment plants [1–3].

Ciprofloxacin (CPX) is a synthetic fluoroquinolone antibiotic widely used in human and veterinary medicine. Concentrations of ciprofloxacin found in water and wastewater are typically  $<1 \mu\text{g}\cdot\text{L}^{-1}$  [4]. Several studies have reported concentrations of 3–87  $\mu\text{g}\cdot\text{L}^{-1}$  in hospital wastewater, and up to 50  $\text{mg}\cdot\text{L}^{-1}$  in wastewater from pharmaceutical production facilities [5]. Their presence in the environment can have adverse effects on water quality and induce the growth of antibiotic-resistant bacteria [4,6]. Therefore, wastewater treatment is necessary in order to remove CPX.

Various treatment methods have been used to remove CPX from aqueous effluents: chemical and electrochemical oxidation, photocatalytic and enzymatic degradation, membrane separation and adsorption [4,7]. Adsorption has proven to be an effective and

promising method due to its simple design and operation, its low cost, the possibility of adsorbent regeneration and its ability to remove low concentrations of micropollutants [8]. The most commonly used adsorbent is activated carbon, although the use of a variety of alternative adsorbents is being investigated. Malakootian et al. (2021) [9] reviewed the removal of CPX via adsorption. Some of the alternative adsorbents studied include zeolites, carbon nanotubes, graphene, nanostructured hybrid materials, clays, magnetic adsorbents, nanoparticles, etc. [1,4,6,9–12].

Due to the high cost of activated carbon, the use of biochar as a solid adsorbent has been of great interest in recent years [13]. Biochar is a carbon-rich material obtained by heating biomass at relatively low temperatures (<700 °C) in an oxygen-poor atmosphere. Biochar is known for its ability to act as a remediator of contaminants, playing an important role in climate change mitigation and bioenergy production [14]. Its high specific surface area, porous structure, surface rich in functional groups and its mineral components make biochar a very good adsorbent for the removal of pollutants present in aqueous solutions [15–19]. The major mechanisms involved in pharmaceutical pollutant adsorption are pore filling, metal complexing, precipitation, hydrogen bonding, ion exchange, cation bridging and hydrophobic partition [20,21]. The behaviour of biochar as an adsorbent depends on the type of raw material and the method used to obtain it (mainly the temperature and residence time) [22,23].

The adsorption performance of raw biochar is limited. This material, typically derived from renewable and low-cost agricultural biomass and solid wastes, can be physically or chemically activated to improve its adsorption properties. As a result, the performance of activated biochar in removing pollutants is comparable to that of commercial activated carbon. The activation of biochar can be carried out via physical methods using steam or gas (CO<sub>2</sub>, N<sub>2</sub>, NH<sub>3</sub>, air, O<sub>2</sub> or their mixtures). Chemical activation can be conducted through treatments with acids (HCl, HNO<sub>3</sub>, H<sub>2</sub>SO<sub>4</sub> or H<sub>3</sub>PO<sub>4</sub>), alkalis (NaOH, KOH or K<sub>2</sub>CO<sub>3</sub>) or oxidants (H<sub>2</sub>O<sub>2</sub> or KMnO<sub>4</sub>) [22]. Several studies have investigated CPX adsorption on raw and activated biochar prepared from different feedstocks: bamboo chips [7], cassava dregs [15], desiccated rice husks [24], used tea leaves [16], potato stems and leaves [17], rice husks [25], rabbit manure [26], municipal solid waste [27], sewage sludge [28], banana peels [29], kidney bean peels, tangerine peels, snowberry, borage and red pepper seeds [30], pumpkin peels [31], etc.

Various by-products and residues are generated during the production of beer. The most abundant by-product is spent grains (bagasse), which is produced after the pressing and filtering of the must from the saccharification of the malted barley grains. It is estimated that the production of 1000 L of beer produces 200 kg of wet spent grains (containing 70–80% water) [32]. The main use of this by-product is its use as animal feed, due to its high protein and fibre content. Spent grains are a carbonaceous material, rich in cellulose, hemicellulose and lignin (together accounting for about 72% (*w/w*) of the dry composition of spent grain) containing large amounts of sugars and numerous phenolic compounds and amino acids [33]. This material has been used as a precursor for various adsorbents for the removal of various drugs in aqueous solutions [34–36]. In this work, bagasse from the brewing industry was used as a feedstock to produce activated biochar (AB) via chemical activation with K<sub>2</sub>CO<sub>3</sub>. The hydrolysis of this activation agent produces KOH, and compared to this, potassium carbonate has the advantage of being less corrosive, easier to store and more environmentally friendly. Furthermore, previous studies have shown that this activation agent is very effective in creating porosity in hydrochar, resulting in materials with large surface areas (>2000 m<sup>2</sup>·g<sup>-1</sup>) and a tenable pore size distribution [37].

The main objective of this research is to study the uptake of CPX from aqueous solutions through sorption on AB. The influence of pH and temperature on adsorption uptake was analysed. Sorption kinetics and equilibrium isotherms were determined, and the sorption mechanism was discussed. Considering the interest of the European biochar certificate in the sustainable use of biochar in Europe, this study can contribute to providing information on the possibility of using waste from the brewing industry as a precursor

of activated biochar for wastewater treatment, specifically for the removal of CPX, an emerging pollutant commonly found in wastewater.

## 2. Materials and Methods

### 2.1. Activated Biochar Preparation

The adsorbent used in this work was biochar activated with potassium carbonate. The biochar was obtained from bagasse, a by-product of the brewing industry. The bagasse, collected from an industry located in the Region of Murcia (Spain), was first dried at 60 °C–70 °C in an oven, and then crushed and sieved, to obtain particles with a size between 1.0 mm and 2.5 mm. This fraction size was pyrolysed in a horizontal rotary quartz furnace (Nabertherm) under an inert argon flow, according to the following steps:

1. Heating from room temperature to 105 °C in 15 min;
2. Holding at 105 °C for 15 min;
3. Heating to 400 °C (5 °C min<sup>-1</sup> heating rate);
4. Holding at 400 °C for 2 h;
5. Cooling to room temperature;
6. The argon flow was 50 L·h<sup>-1</sup> in the 1st, 2nd and 5th stages, and 150 L·h<sup>-1</sup> in the 3rd and 4th stages.

The pyrolysis conditions were set, taking into account those reported in the literature for similar studies. Thus, the treatment at 400 °C with a ramp of 5 °C·min<sup>-1</sup> is common in the production of biochar from different types of biomass, as these conditions fall within the range used to favour the production of biochar over the production of bio-oil and gasification [38,39]. Furthermore, these particle size and pyrolysis conditions have previously been used to produce biochar for soil remediation and have shown good performance in terms of biochar production [40].

The resulting biochar was then crushed, sieved and activated via an alkaline treatment with K<sub>2</sub>CO<sub>3</sub>. A total of 5.0 g of biochar (particle size between 0.15 mm and 0.5 mm) was suspended in 100 mL of a 2 mol·L<sup>-1</sup> K<sub>2</sub>CO<sub>3</sub> solution with continuous stirring. After 24 h, the suspension was centrifuged, and the solid was dried at 105 °C, placed in lidded porcelain crucibles and heated in a muffle furnace at 800 °C for 3 h. Finally, the activated biochar was repeatedly washed with distilled water to a stable pH (pH ≈ 7) and dried at 60 °C–70 °C. These impregnation and carbonisation conditions are within the normal range used for the alkaline activation of other biochars derived from other low-cost materials [41,42]. At high activation temperatures (600 °C–800 °C), potassium carbonate catalyses the gasification of cellulose, which is more complete at higher temperatures. Thus, the use of potassium carbonate as an activation agent at high temperatures produces biochar with high porosity and a high specific surface area, which facilitates the diffusion of adsorbates and increases their adsorption capacity [42,43].

### 2.2. Activated Biochar Characterization

Fourier Transform Infrared Spectroscopy (FTIR) and the point of zero charge were used to characterize the AB sorbent.

FTIR is a commonly used technique to identify surface functional groups on sorbents. For this purpose, FTIR spectra (Perkin Elmer 16F PC) of AB samples were obtained before and after CPX adsorption. The samples were prepared as KBr discs, and the spectra were recorded in the range of 650–4000 cm<sup>-1</sup>.

The electrical charge on the surface of a sorbent is zero at the point of zero charge. This parameter is usually considered as the pH (pH<sub>pzc</sub>) at which a solid immersed in an electrolyte has a net zero electrical charge on the surface.

The point of zero charge was determined using two classical methods: the immersion technique and mass titrations.

In the immersion technique [44], 20 mL of a 0.01 M NaCl solution were placed in different flasks, and the pH was adjusted to values between 3 and 9.5 by adding NaOH or HCl solutions. Then, 20 mg of AB were added to each flask, and the suspensions were

shaken for 24 h until the equilibrium pH was reached ( $\text{pH}_{\text{final}}$ ). Blank tests were made without AB samples and their pH was measured after 24 h, referred to as  $\text{pH}_{\text{initial}}$ . The  $\text{pH}_{\text{pzc}}$  value is the point where the  $\text{pH}_{\text{initial}} = \text{pH}_{\text{final}}$  in the plot of  $\text{pH}_{\text{final}}$  vs.  $\text{pH}_{\text{initial}}$ .

In the mass titration method [45], 5 mL of a 0.01 M NaCl solution were added to each of several flasks. Different amounts of solid AB were added to each flask to obtain solid suspensions with concentrations between 2 and 80  $\text{g}\cdot\text{L}^{-1}$ . After 24 h of agitation, the pH of the suspensions was measured. Plotting the equilibrium pH versus the sorbent concentration achieves a plateau corresponding to the  $\text{pH}_{\text{pzc}}$  value.

### 2.3. CPX Solutions' Preparation and Analysis

Ciprofloxacin ( $\text{C}_{17}\text{H}_{18}\text{FN}_3\text{O}_3$ ) with >98% purity was supplied by Sigma-Aldrich. The molecular weight of CPX is 331.35  $\text{g}\cdot\text{mol}^{-1}$ , and its molecule has two dissociation constants:  $\text{pK}_{\text{a}1} = 5.9 \pm 0.15$  corresponding to the carboxyl group, and  $\text{pK}_{\text{a}2} = 8.89 \pm 0.11$  for the amine group in the piperazine moiety. As a function of pH, the CPX molecule exists in different ionic forms: the cationic form predominates when the pH is below 5.9, the zwitterionic form predominates when the pH is between 5.9 and 8.89 and the anionic form predominates when the pH is above 8.89 [1,24,46] (Supplementary Figure S1).

A CPX stock solution (1000  $\text{mg}\cdot\text{L}^{-1}$ ) was prepared by dissolving 1 g of CPX in 1 L of 0.1 M HCl. Working solutions of different CPX concentrations were obtained by diluting the CPX stock solution with distilled water. The pH of the solutions was adjusted through the addition of 0.1 M NaOH or  $\text{HNO}_3$  solutions, if necessary. The concentration of CPX in the solutions was measured via UV spectrophotometry (Shimadzu UV-1603 UV-visible spectrophotometer). The wavelength at which the maximum absorbance occurred in the CPX solutions was pH-dependent:  $\lambda_{\text{max}} = 277.5$  nm at acidic pH and  $\lambda_{\text{max}} = 272$  nm at basic pH (absorption spectra of CPX solutions at acidic or basic pH are shown in the Supplementary Figure S2). Two calibration curves were obtained, one at  $\lambda = 277.5$  nm for acidic solutions and other one at  $\lambda = 272$  nm for basic solutions, both with regression coefficients greater than 0.999. From each of these calibration curves, the limit of detection (LOD) and limit of quantitation (LOQ) were obtained according to IUPAC and ACS recommendations, respectively [47,48]. The limits obtained under acidic conditions were  $\text{LOD} = 0.70$   $\text{mg}\cdot\text{L}^{-1}$  and  $\text{LOQ} = 2.34$   $\text{mg}\cdot\text{L}^{-1}$ , and those obtained under basic conditions were  $\text{LOD} = 0.72$   $\text{mg}\cdot\text{L}^{-1}$  and  $\text{LOQ} = 2.40$   $\text{mg}\cdot\text{L}^{-1}$ .

### 2.4. Adsorption Experiments

To determine the influence of pH and temperature on the sorption process, and to study the kinetic and the equilibrium of the CPX adsorption, batch adsorption experiments were carried out, at a constant temperature and pH, in magnetically stirred glass flasks. Typically, known amounts of sorbent were placed in contact with a CPX solution of a known concentration. The pH of the suspension was maintained at the desired value by adding dilute solutions of  $\text{HNO}_3$  or NaOH. At specified times, suspension samples were collected and centrifuged, and the supernatant was analysed for CPX determination. The amount of CPX adsorbed per unit of adsorbent,  $q$  ( $\text{mg CPX}\cdot\text{g}^{-1}$ ), was obtained from Equation (1).

$$q = \frac{C_0 \cdot V_0 - C \cdot V}{m} \quad (1)$$

where  $C_0$  and  $C$  are the initial CPX concentration in the solution and that at time  $t$  ( $\text{mg}\cdot\text{L}^{-1}$ ), respectively;  $V_0$  and  $V$  are the initial solution volume and that at time  $t$  (L); and  $m$  is the mass (g) of sorbent used.

The tests were carried out in triplicate with a sorbent dose of 0.5  $\text{g}\cdot\text{L}^{-1}$  in all cases. Blank tests were also performed by contacting the solid adsorbent with distilled water, which showed that the absorbance of the solutions obtained was negligible at  $\lambda = 277.5$  nm and 272 nm.

The influence of pH on CPX adsorption was investigated at 25 °C by mixing 0.025 g of the sorbent with 50 mL of the 300 mg·L<sup>-1</sup> CPX solution for 72 h at a pH adjusted between 2 and 10.5. Blank tests were performed without the sorbent at the same pH values.

The effect of temperature was studied at pH 3.5 by contacting 0.025 g of sorbent with 50 mL of the 300 mg·L<sup>-1</sup> CPX solution for 72 h. The tests were carried out at 10 °C, 25 °C, 40 °C and 55 °C.

The adsorption kinetic was determined at 25 °C and pH 3.5. The solid adsorbent (0.1 g) was added to 200 mL of the 300 mg·L<sup>-1</sup> CPX solution, and suspension samples were periodically taken and analysed. Different kinetic models (pseudo-first- and pseudo-second-order, Elovich, intraparticle diffusion and Bangham) were used to obtain information on the adsorption mechanism (Table 1) [49].

**Table 1.** Kinetic adsorption models.

Kinetic Model	Equation	Parameters
Pseudo-first order	$q_t = q_e \cdot (1 - e^{-k'_1 \cdot t})$	$q_e$ , amount of adsorbate sorbed at equilibrium (mg·g <sup>-1</sup> ) $k'_1$ , adsorption rate constant (min <sup>-1</sup> )
Pseudo-second order	$q_t = \frac{t}{\frac{1}{k'_2 \cdot q_e^2} + \frac{t}{q_e}}$	$q_e$ , amount of adsorbate sorbed at equilibrium (mg·g <sup>-1</sup> ) $k'_2$ , adsorption rate constant (g·mg <sup>-1</sup> ·min <sup>-1</sup> ) $h = k'_2 \cdot q_e^2$ , initial adsorption rate (mg·g <sup>-1</sup> ·min <sup>-1</sup> )
Elovich equation	$q_t = \frac{1}{\beta} \cdot \ln(\alpha \cdot \beta) + \frac{1}{\beta} \cdot \ln t$	$\alpha$ , initial adsorption rate (mg·g <sup>-1</sup> ·min <sup>-1</sup> ) $\beta$ , constant related to the extend of surface coverage and activation energy for chemisorption (g·mg <sup>-1</sup> )
Intraparticle diffusion	$q_t = k_d \cdot t^{1/2} + C$	$k_d$ , rate constant (mg·g <sup>-1</sup> ·min <sup>-1/2</sup> ) $C$ , constant related with the thickness of boundary layer (mg·g <sup>-1</sup> )
Bangham	$\log \left\{ \log \left( \frac{C_0}{C_0 - q_t \cdot m/V} \right) \right\} = \log \left( \frac{k_B \cdot m/V}{2.303} \right) + \sigma \log(t)$	$k_B$ , constant parameter (L·g <sup>-1</sup> ) $\sigma$ , constant parameter (<1)

The adsorption isotherm was obtained at 25 °C and pH 3.5. A total of 0.025 g of the sorbent and 50 mL of the CPX solutions with concentrations ranging from 25 mg·L<sup>-1</sup> to 1000 mg·L<sup>-1</sup> were mixed in glass flasks until equilibrium was reached (≈80 h). The Langmuir, Freundlich, Sips, Redlich–Peterson and Toth isotherm models were used to understand the adsorption interactions (Table 2) [50].

**Table 2.** Isotherm models.

Isotherm Model	Equation	Parameter
Langmuir	$q_e = \frac{q_{mL} \cdot K_L \cdot C_e}{1 + K_L \cdot C_e}$	$q_{mL}$ , maximum sorption capacity (mg·g <sup>-1</sup> ) $K_L$ , Langmuir isotherm constant (L·mg <sup>-1</sup> ).
Freundlich	$q_e = K_F \cdot C_e^{1/n}$	$K_F$ , Freundlich isotherm constant ((mg·g <sup>-1</sup> )(mg·L <sup>-1</sup> ) <sup>-1/n</sup> ) $n$ , Freundlich isotherm exponent constant
Sips	$q_e = \frac{q_{mS} \cdot K_S \cdot C_e^{1/n_S}}{1 + K_S \cdot C_e^{1/n_S}}$	$q_{mS}$ , maximum sorption capacity (mg·g <sup>-1</sup> ) $K_S$ , Sips isotherm constant, (L <sup>1/n_S</sup> ·mg <sup>-1/n_S</sup> ) $n_S$ , Sips isotherm exponent
Redlich–Peterson	$q_e = \frac{K_R \cdot C_e}{1 + a_R \cdot C_e^\beta}$	$K_R$ , Redlich–Peterson isotherm constant (L·g <sup>-1</sup> ) $a_R$ , Redlich–Peterson isotherm constant (L <sup>β</sup> ·mg <sup>-β</sup> ) $\beta$ , Redlich–Peterson isotherm exponent
Toth	$q_e = \frac{q_{mT} \cdot C_e}{(1/K_T + C_e^{T_T})^{1/T_T}}$	$q_{mT}$ , maximum sorption capacity (mg·g <sup>-1</sup> ) $K_T$ , constant that characterize the adsorptive potential ((L·g <sup>-1</sup> ) <sup>T_T</sup> ) $T_T$ , Toth parameter related to the heterogeneity of the adsorbent (dimensionless)

The kinetic models and the equilibrium isotherms were fitted to the corresponding experimental data using non-linear regression with the Solver add-in of Microsoft Excel, minimising the ARE function (average relative error, %) (Equation (2)).

$$\text{ARE (\%)} = \frac{100}{p} \cdot \sum_{i=1}^p \left( \frac{|q_{\text{exp}} - q_{\text{cal}}|}{q_{\text{exp}}} \right)_i \quad (2)$$

where  $p$  is the number of data,  $q_{\text{exp}}$  is the experimental amount of CPX adsorbed per unit of adsorbent and  $q_{\text{cal}}$  is the amount of CPX adsorbed per unit of adsorbent provided by the model.

### 3. Results and Discussion

#### 3.1. Activated Biochar Characterization and Adsorption Mechanism

Figure 1 shows the FTIR spectra of the adsorbent before and after CPX adsorption. Both spectra are very similar, and the same spectral peaks can be observed. No significant changes in the peak profile can be detected after CPX adsorption. The high number of adsorption peaks highlights the complexity of the activated biochar. An intense absorption peak at  $3434 \text{ cm}^{-1}$  can be clearly identified, corresponding to the stretching vibrations of the O-H of the free hydroxyl groups (alcohols and phenols) and the bonded OH bands of carboxylic acids. Also, the presence of adsorbed water molecules from atmospheric humidity may influence the intensity and amplitude of this band [51,52].

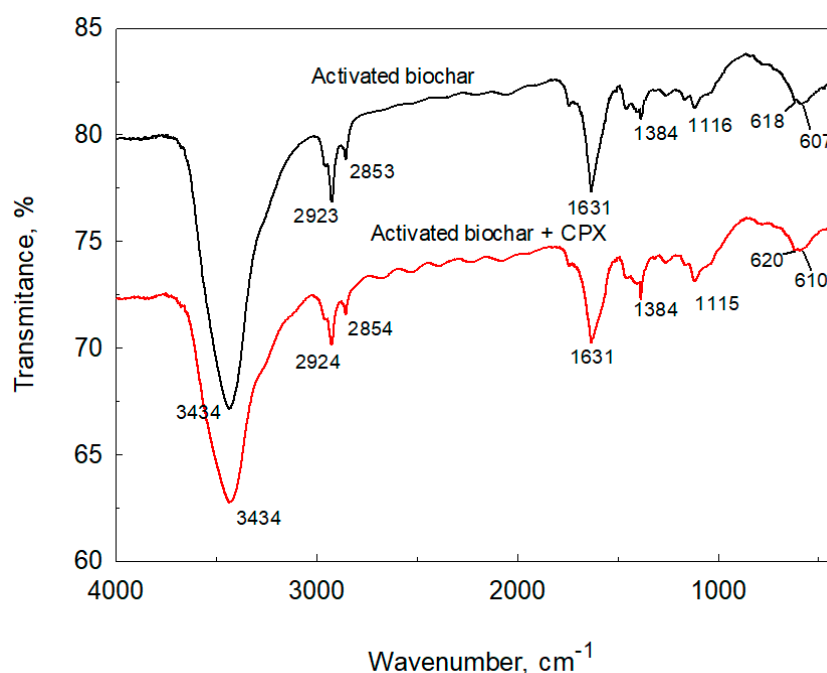


**Figure 1.** FTIR spectra of activated biochar before and after CPX adsorption.

The peak at  $2923 \text{ cm}^{-1}$  can be attributed to the asymmetric stretching of C-H in aliphatic groups. The peak at  $2853 \text{ cm}^{-1}$  can be attributed to the symmetric stretching of C-H in aliphatic groups, and to the methoxy group ( $\text{CH}_3\text{-O}$ ). The band at  $1631 \text{ cm}^{-1}$  shows the asymmetric stretching of  $\text{COO}^-$ , the C=C stretching that can be attributed to the presence of aromatic rings, and the bending vibration of the interlayer water molecules [52]. The peak at  $1384 \text{ cm}^{-1}$  corresponds to the symmetric stretching of  $\text{COO}^-$  or S=O in sulphonyl and sulphonate. The peak at  $1115 \text{ cm}^{-1}$ , in the range of  $1050\text{--}1150 \text{ cm}^{-1}$ , can be attributed to the C-O stretching vibration in carboxylic acids, ethers and alcohols [10,16,53]. Therefore, biochar presents an abundant number of surface functional groups such as hydroxyl,

methyl, carbonyl and carboxyl groups; the C=C bonds and C-H groups of the aromatic rings may be implicated in the adsorption of CPX by AB.

The experimental values corresponding to the mass titration and immersion techniques are shown in Figure 2. The  $\text{pH}_{\text{pzc}}$  obtained by these two methods was  $\approx 8.1$ , slightly basic, according with the activation method used (with  $\text{K}_2\text{CO}_3$ ). The solid surface therefore has a basic character.

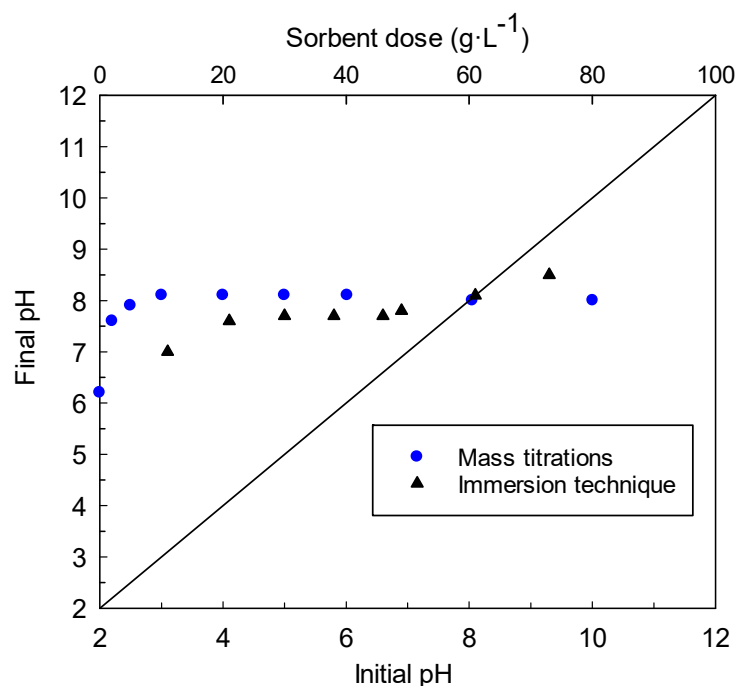


**Figure 2.** Determination of activated biochar's point of zero charge.

The adsorption of organic pollutants onto biochar can involve different mechanisms such as pore filling, hydrophobic interaction, partitioning, hydrogen bonds, van der Waals forces, electrostatic interaction and  $\pi$ - $\pi$  interactions [8,21]. The mechanisms implicated in the adsorption of CPX on biochar are complex due to the chemical structure of the CPX molecule, with several aromatic rings and ionisable functional groups, and the heterogeneous nature of the adsorbent solid. Nevertheless, it can be suggested that several possible mechanisms are involved: electrostatic attraction, hydrogen bonding and  $\pi$ - $\pi$  interactions.

Electrostatic interactions can occur between the functional groups of the activated biochar and the CPX molecules. In this sense, the solution pH plays an important role, since both the ionic form of CPX and the charge on the AB surface are affected by this parameter. The tests were carried out at pH 3.5 to avoid CPX removal via precipitation. At this pH, which is lower than  $\text{pH}_{\text{pzc}}$ , the sorbent surface is positively charged and the predominant ionic form of CPX is the cationic one. Therefore, the contribution of this mechanism to the overall adsorption process should be slight, and there must be other different mechanisms than electrostatic attraction involved in CPX adsorption by AB [45].

Adsorption may also involve hydrogen-bond interactions. The CPX molecule contains several moieties such as aromatic rings, as well as nitrogen, fluorine and oxygen atoms that may interact through H-bonds with the aromatic rings and other groups (such as -OH and COOH) on the surface of AB.

Taking into account the presence of phenolic groups and aromatic rings on the AB surface, it can be suggested that there may be  $\pi$ - $\pi$  interactions implicated in the adsorption process. This type of interaction may contribute significantly to the adsorption of organic pollutants possessing aromatic rings. The  $\pi$ - $\pi$  interaction occurs between electron-poor and electron-rich structures. The CPX molecule possesses aromatic rings connected to O, N and F atoms. These atoms are highly electronegative and have a high electron-holding ability.

This will make the aromatic rings electron-deficient, acting as electron acceptors. The hydroxyl groups and the C=C bonding of the aromatic rings on the adsorbent surface make them electron donors. Consequently, an electron donor/acceptor adsorption mechanism based on the non-uniform distribution of electrons between the adsorbate molecule and the functional groups of the adsorbent may contribute to the adsorption of CPX on AB.

So, it can be hypothesised that hydrogen bonding and  $\pi$ - $\pi$  interactions may be involved in the adsorption of CPX onto AB.

### 3.2. Effect of pH and Temperature on CPX Adsorption

The amount of CPX adsorbed per unit of adsorbent is usually significantly affected by the pH of the solution, which affects the chemical form of the adsorbate (anionic, cationic or molecular forms) and the surface properties (surface functional groups, charge and charge density) of the adsorbent solid. Figure 3 shows the removal efficiency of CPX vs. the pH of the solution at equilibrium in tests carried out with and without (blank trials) the solid adsorbent.

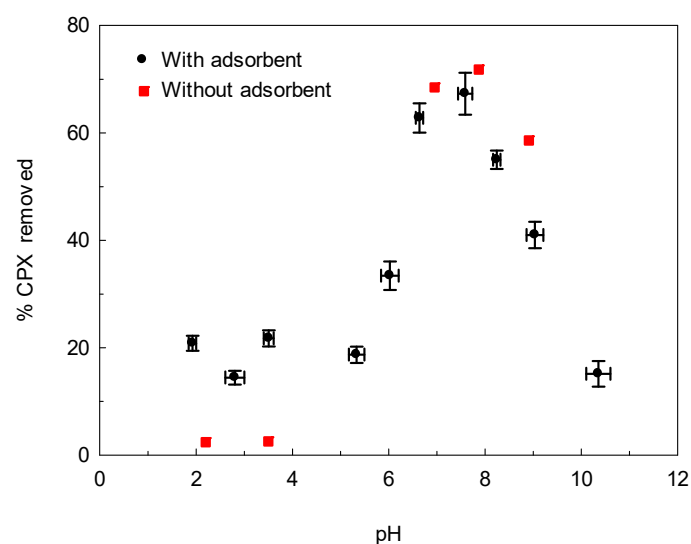


**Figure 3.** Effect of pH on CPX adsorption at equilibrium. The symbols are the average values, and the upper and lower bars indicate the standard deviation. Conditions: temperature = 25 °C; contact time = 72 h; sorbent dose = 0.5 g·L<sup>-1</sup>; C<sub>0</sub> CPX = 300 mg·L<sup>-1</sup>.

In the assays performed at pH 6 to 10, turbidity was observed in the solutions, indicating that CPX precipitation occurred. For this reason, blank assays (without adsorbent) were performed. It was observed that the percentage of CPX removal at pH 7 to 9 was very similar in the assays carried out with and without the adsorbent. Therefore, the increase in CPX removal observed at these pH values was mainly due to precipitation rather than adsorption.

As mentioned above, CPX can exist in different forms depending on the pH value. At pH values less than 5.9, the dominant form in the solution is cationic CPX (CPX<sup>+</sup>). At pH values above 8.9, the predominant form is anionic CPX (CPX<sup>-</sup>). The solubilities of these net-charged species (CPX<sup>+</sup> and CPX<sup>-</sup>) are high, being higher at pH values below 5 (>30 g·L<sup>-1</sup>). At pH values between 5.9 and 8.9, the zwitterionic form predominates, and the solubility of this neutral species is very low (<0.12g·L<sup>-1</sup>) [1,24,46]. Therefore, the following experiments were performed at pH 3.5 in order to minimise the removal of CPX via precipitation.

The amount of CPX adsorbed per unit of adsorbent was obtained at different temperatures. It was found that the  $q_e$  values increased with increasing temperatures (34.6 mg·g<sup>-1</sup> at 10 °C, 41.4 mg·g<sup>-1</sup> at 25 °C, 89.3 mg·g<sup>-1</sup> at 40 °C and 109.9 mg·g<sup>-1</sup> at 55 °C). According to these results, it can be stated that adsorption was favoured as the temperature increased,

showing the endothermicity of this process. This fact is in agreement with the investigations of CPX adsorption on different sorbents reviewed by Malakootian et al. (2021) [9]. This process is endothermic in 66% of the papers investigating the thermodynamics of CPX adsorption and in all those where the sorbent used is biochar: rabbit manure biochar [26], a magnetic biochar-based manganese oxide composite [18], potassium hydroxide-modified biochar derived from potato stems and leaves [17] and a coating of magnetic biochar with humic acid [54]. However, CPX adsorption was exothermic on biochar prepared from cassava dregs [15] and both exothermic and endothermic on biochar obtained from used tea leaves [16].

### 3.3. Adsorption Kinetics

The study of the adsorption kinetics is of great importance for the prediction of the rate at which CPX will be removed and for the design of the appropriate adsorption equipment. Figure 4 shows the experimental values of CPX adsorbed per gram of adsorbent ( $q_t$ ) vs. contact time. As can be seen, the adsorption process takes place in several steps. Initially, in the first step, the  $q_t$  values increase sharply with the contact time because the system is far from equilibrium and many binding sites are available on the external surface and in the macropores. Then, the sorption rate decreases because there are fewer sorption sites available, and the CPX concentration gradient decreases as the system evolves towards equilibrium. More than 3 days of contact time were required to reach the equilibrium. The contact time required to reach equilibrium varies widely depending on the nature of the adsorbate and adsorbent, the adsorbent particle size and the initial adsorbate concentrations. Reported equilibrium times for the adsorption of CPX include three days for adsorption on activated carbon, carbon xerogel and carbon nanotubes [1]; over five days for an initial concentration of  $842 \text{ mg}\cdot\text{L}^{-1}$  and over two days for  $84.2 \text{ mg}\cdot\text{L}^{-1}$  for adsorption on bamboo-based activated carbon [7]; more than 24 h for adsorption on biochar from cassava dregs [15]; over nine hours with biochar from used tea leaves [16]; and 24 h for adsorption on pumpkin peel biochar prepared with phosphoric acid [31].

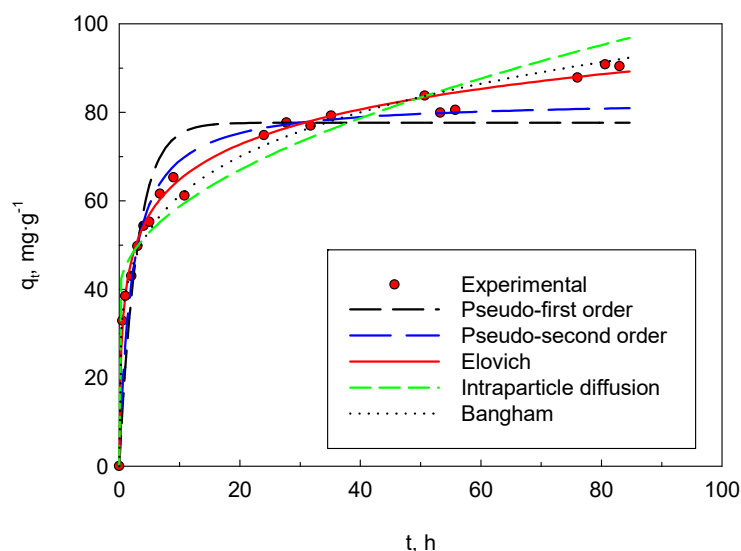


**Figure 4.** CPX adsorption kinetics onto activated biochar. Conditions: temperature =  $25 \text{ }^\circ\text{C}$ ; pH = 3.5; sorbent dose =  $0.5 \text{ g}\cdot\text{L}^{-1}$ ;  $C_0$  CPX =  $300 \text{ mg}\cdot\text{L}^{-1}$ .

There are several steps involved in the adsorption of a solute onto the surface of an adsorbent solid: (1) adsorbate movement from the fluid phase to the boundary layer next to the adsorbent surface, (2) adsorbate diffusion through the boundary layer to the outer adsorbent surface, (3) adsorption on the active sites on the adsorbent surface, (4) the diffusion of the adsorbate into the pores of the adsorbent, and (5) adsorption on the active

sites inside the pores. The overall rate at which adsorption occurs may be controlled by one or more of these steps.

To study the adsorption mechanism and establish the rate-controlling steps, the experimental data have been fitted to five kinetic models: pseudo-first order, pseudo-second order, Elovich, intraparticle diffusion and Bangham (Table 1). The fit to the kinetic models is shown in Figure 4 and the obtained characteristic parameters are listed in Table 3.

**Table 3.** Kinetic parameters for the sorption of CPX by AB.

Pseudo-First Order		Pseudo-Second Order		Elovich		Intraparticle Diffusion		Bangham	
$q_e$ ( $\text{mg}\cdot\text{g}^{-1}$ )	77.7	$q_e$ ( $\text{mg}\cdot\text{g}^{-1}$ )	82.92	$\alpha$ ( $\text{mg}\cdot\text{g}^{-1}\cdot\text{min}^{-1}$ )	5.50	$k_d$ ( $\text{mg}\cdot\text{g}^{-1}\cdot\text{min}^{-0.5}$ )	0.81	$k_B$ ( $\text{L}\cdot\text{g}^{-1}$ )	0.059
$k'_1$ ( $\text{min}^{-1}$ )	0.0057	$k'_2$ ( $\text{g}\cdot\text{mg}^{-1}\cdot\text{min}^{-1}$ )	0.0001	$\beta$ ( $\text{g}\cdot\text{mg}^{-1}$ )	0.087	$C$ ( $\text{mg}\cdot\text{g}^{-1}$ )	38.81	$\sigma$	0.21
ARE (%)	12.40	ARE (%)	7.62	ARE (%)	2.52	ARE (%)	7.33	ARE (%)	3.17

A frequently used kinetic model to study the mechanism of diffusion during adsorption is intraparticle diffusion [6,16]. As can be observed in Figure 4, this model does not adequately describe the adsorption kinetics of CPX on AB (ARE = 7.3%) over the entire experimental period. A plot of  $q_t$  versus  $t^{1/2}$  is shown in Figure 5. As can be seen, the overall adsorption process can be divided into two linear zones. This suggests that the rate of adsorption is controlled by several steps, and not only by intraparticle diffusion. The first linear zone has the steepest slope and is related to the diffusion of CPX through the boundary layer to the outer surface of the AB. Moreover, this first linear zone does not pass through the coordinate origin, suggesting that the adsorption rate at this initial stage is influenced by diffusion through the boundary layer. The second linear zone is related to intraparticle diffusion in the micropores and mesopores of the AB. The lower slope of this second zone indicates that there is a higher mass transfer resistance at this stage, and that CPX diffusion into the pores of AB is a slower process.

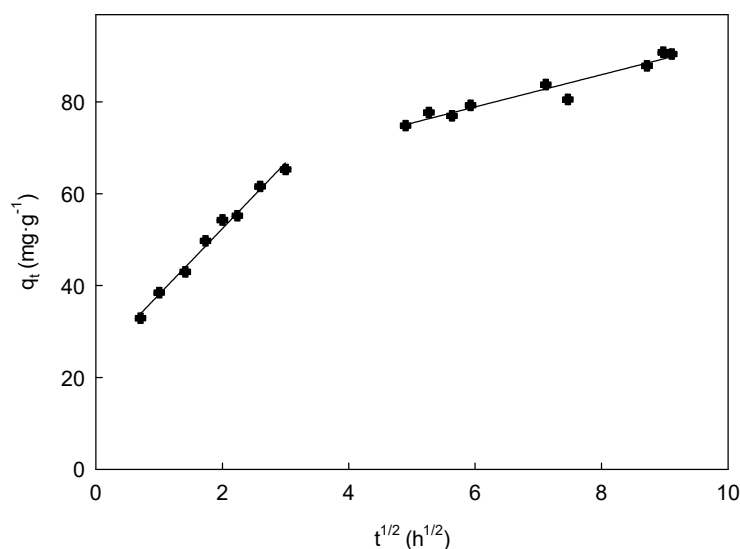


**Figure 5.** CPX intraparticle diffusion model. Conditions: temperature = 25 °C; pH = 3.5; sorbent dose = 0.5  $\text{g}\cdot\text{L}^{-1}$ ;  $C_0$  CPX = 300  $\text{mg}\cdot\text{L}^{-1}$ .

Thus, it can be indicated that the overall adsorption process is complex and involves both diffusion of CPX through the boundary layer and intraparticle diffusion in the AB pores.

Based on the lowest ARE values, it can be said that the Elovich and Bangham models adjusted the experimental data better than the other used models, and the sorption process can be described adequately by those two models (ARE values lower than 3.2%). The

good fitting to the Elovich and Bangham models suggests the presence of the chemical adsorption of CPX on a heterogeneous sorbent surface, and that the limiting stage is the solute's diffusion within the pores [46,49].

### 3.4. Effect of Initial Concentration and Adsorption Isotherm

The influence of the initial CPX concentrations, ranging from 35 mg·L<sup>-1</sup> to 925 mg·L<sup>-1</sup>, on the adsorption capacity and removal percentage was studied (Figure 6). An increase in the initial concentration leads to an increase in the adsorption capacity due to the increased concentration gradient between the solution and the adsorbent, while the removal percentage decreases because the number of available active sites remains constant and the competition for these sites increases.

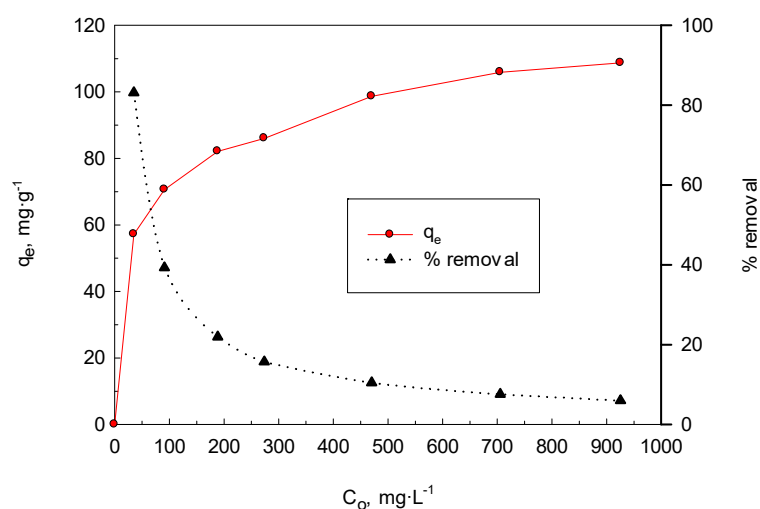


**Figure 6.** Influence of initial concentration on CPX adsorption. Conditions: temperature = 25 °C; pH = 3.5; contact time  $\approx$  80 h; sorbent dose = 0.5 g·L<sup>-1</sup>; C<sub>0</sub> CPX from 25 mg·L<sup>-1</sup> to 1000 mg·L<sup>-1</sup>.

The experimental sorption isotherm (relationship between the concentration of CPX in a solution, C<sub>e</sub>, and the amount of CPX adsorbed per unit adsorbent, q<sub>e</sub>, at equilibrium) at 25 °C is shown in Figure 7. At low C<sub>e</sub> values (C<sub>e</sub> values between 0 and 150 mg·L<sup>-1</sup>), the sorption capacity increases significantly with increasing C<sub>e</sub>. Subsequently the q<sub>e</sub> values tend to reach a constant value, which is the maximum adsorption capacity (approximately 110 mg·g<sup>-1</sup>), although a plateau is not reached even at higher concentrations of CPX in the solution.

Five isotherm models have been used to fit the experimental equilibrium data: Langmuir, Freundlich, Sips, Redlich–Peterson and Toth. The fitted isotherm models are shown in Figure 7. The corresponding characteristic parameters and the ARE values were obtained (Table 4).

**Table 4.** Isotherm parameters for the sorption of CPX by AB.

Langmuir	Freundlich	Sips	Redlich–Peterson	Toth
q <sub>mL</sub> (mg·g <sup>-1</sup> )	K <sub>F</sub> ((mg·g <sup>-1</sup> )(mg·L <sup>-1</sup> ) <sup>-1/n</sup> )	q <sub>mS</sub> (mg·g <sup>-1</sup> )	K <sub>R</sub> (L·g <sup>-1</sup> )	q <sub>mT</sub> (mg·g <sup>-1</sup> )
104.9	38.02	133.4	78.07	131.4
K <sub>L</sub> (L·mg <sup>-1</sup> )	n	K <sub>S</sub> (L <sup>1/ns</sup> ·mg <sup>-1/ns</sup> )	a <sub>R</sub> (L·mg <sup>-1</sup> ) <sup>β</sup>	K <sub>T</sub> (L·mg <sup>-1</sup> ) <sup>Γ</sup>
0.037	6.44	0.43	1.98	2.49
		n <sub>S</sub>	β	T <sub>T</sub>
		3.24	0.85	0.27
ARE (%)	ARE (%)	ARE (%)	ARE (%)	ARE (%)
11.94	2.44	4.92	3.31	5.40

As can be observed, the Freundlich model represents the equilibrium data very well and provides the best fit (lower ARE value, 2.4%). The Redlich–Peterson, Sips and Toth models are also suitable for describing the adsorption process, with ARE values of 3.3%,

4.9% and 5.4%, respectively. The Langmuir model is not suitable to describe CPX adsorption due to the high ARE value (11.9%).

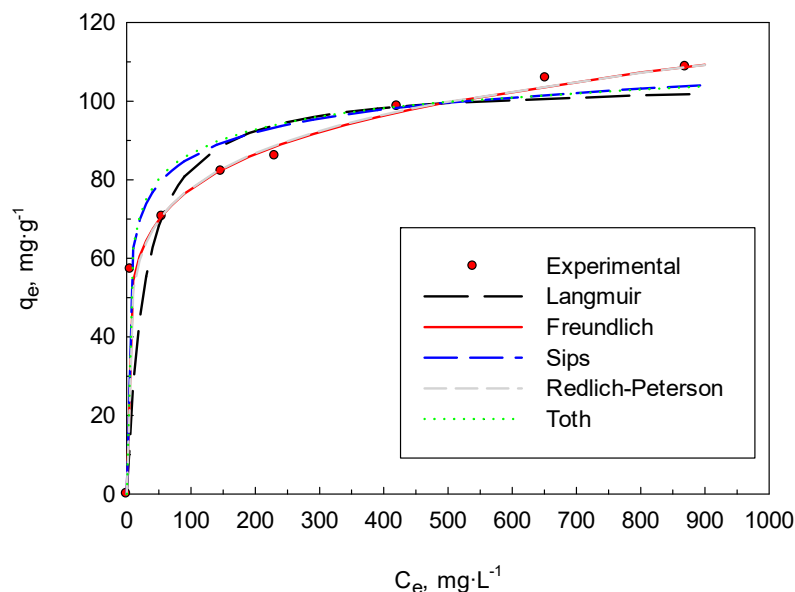


**Figure 7.** Experimental data and predicted isotherms of CPX adsorption on activated biochar. Conditions: temperature = 25 °C; pH = 3.5; contact time  $\approx$  80 h; sorbent dose = 0.5 g·L<sup>-1</sup>; C<sub>0</sub> CPX from 25 mg·L<sup>-1</sup> to 1000 mg·L<sup>-1</sup>.

The best fit to the Freundlich model suggests a multilayer adsorption on a heterogeneous sorbent surface. The low value of the Toth isotherm exponent ( $T_T = 0.27$ ) is in agreement with this statement.

The  $K_F$  value (38.02 (mg·g<sup>-1</sup>) (mg·L<sup>-1</sup>)<sup>-1/n</sup>) is related to the adsorption capacity. The  $n$  parameter is related to the intensity of adsorption, and if its value is greater than one, the adsorption is favourable [53]. The obtained  $n$  value is 6.44, indicating that the sorption of CPX on this activated biochar is favourable.

The constant ( $\beta$ ) of the Redlich–Peterson model and the equilibrium parameter or Hall separation factor ( $R_L$ ), calculated (Equation (3)) from the Langmuir model, are related to the feasibility of the adsorption process.

$$R_L = \frac{1}{1 + K_L \cdot C_0} \quad (3)$$

Adsorption is favourable for  $\beta$  and  $R_L$  values between 0 and 1. In this study, the  $\beta$  value is 0.85 and the calculated  $R_L$  values range from 0.03 to 0.44, indicating that CPX sorption on potassium carbonate activated biochar is favourable, as indicated by the  $n$  parameter of the Freundlich model. Furthermore, the adsorption is enhanced as the initial CPX concentration increases, as shown by the decrease in the  $R_L$  value with increasing initial CPX concentrations.

The value of the Sips isotherm exponent,  $n_S$ , is 3.24. Values of  $n_S$  greater than 1 indicate that the behaviour of the Sips isotherm corresponds to the Freundlich model, and it qualitatively shows the heterogeneity of the adsorbent surface.

The values of the maximum adsorption capacity ( $q_{max}$ ) obtained from the Sips and Toth models are 133.4 mg·g<sup>-1</sup> and 131.4 mg·g<sup>-1</sup>, respectively. Although the Langmuir model gives the worst fit to the experimental data, it can roughly estimate the  $q_{max}$  of the sorbent (104.9 mg·g<sup>-1</sup>). This value is similar to that expected from the experimental data (Figure 7). This value can be compared with other values of maximum adsorption capacity reported in the review by Malakootian et al. (2021) [9] for the adsorption of CPX on different sorbents. These values range from 47 ng·g<sup>-1</sup> (birnessite) to 1575 mg·g<sup>-1</sup> (C@silica

core/shell nanoparticles of ZIF-8). When the sorbent is raw or activated biochar, the  $q_{\max}$  varies between  $8.3 \text{ mg}\cdot\text{g}^{-1}$  (magnetic biochar based on a manganese oxide composite) and  $449.4 \text{ mg}\cdot\text{g}^{-1}$  (magnetic biochar doped with ZnO from camphor leaves). For comparison, Table 5 shows typical values for the maximum sorption capacity of some biochars recently used for CPX removal. As can be seen, the  $\text{K}_2\text{CO}_3$ -activated biochar prepared from barley bagasse has an adsorption capacity intermediate between those reported for other biochars.

**Table 5.** CPX maximum adsorption capacities of various raw and modified biochars.

Adsorbent	$q_{\max}$ ( $\text{mg}\cdot\text{g}^{-1}$ )	Reference
Magnetic biochar-based manganese oxide composite	8.3	[18]
KOH-activated potato stems and leaves biochar	8.8	[17]
Banana peel biochar	21.0	[29]
Rice husk biochar	36.1	[25]
Sewage sludge biochar	46.2	[28]
Rabbit manure biochar	70.2	[26]
Fe/Zn magnetic sludge biochar	74.2	[55]
$\text{K}_2\text{CO}_3$ -activated barley bagasse biochar	104.9	This study
HCl-activated clay/coconut husk	139.9	[56]
Phosphoric acid-activated pumpkin peel biochar	153.9	[31]
Municipal solid waste biochar–montmorillonite composite	167.4	[27]
KOH-activated clay/coconut husk	228.7	[56]
Graphene hydrogel	235.7	[12]
Tea leaf biochar	238.1	[16]
$\text{Fe}_3\text{O}_4$ /graphene oxide/citrus peel-derived biochar-based nanocomposite	283.4	[57]
Magnetic ZnO-doped camphor leaf biochar	449.4	[58]

#### 4. Conclusions

Activation with  $\text{K}_2\text{CO}_3$  and the subsequent calcination at  $800^\circ\text{C}$  of biochar produced from the pyrolysis of barley bagasse from the brewing industry improved its adsorption properties. The activated biochar was characterised using FTIR, and its  $\text{pH}_{\text{pzc}}$  was determined. The adsorption capacity of this material was tested with CPX, a widely used antibiotic. The peak profile of the FTIR spectra of the sorbent, before and after CPX adsorption, are very similar. The zero-charge sorption point is weakly basic ( $\text{pH}_{\text{pzc}} \approx 8.1$ ) according to the activation method. It has been observed that precipitation of CPX occurs at pH values between 6 and 9, so it is convenient to perform adsorption under acidic conditions to minimise CPX precipitation. The amount of CPX adsorbed per unit of adsorbent increases with increasing temperature, reflecting the endothermicity of the process. The adsorption kinetic is slow, and after 24 h of contact, 82% of the amount adsorbed at equilibrium is adsorbed. The Elovich and Bangham kinetic models adequately describe the kinetics of the process. With respect to the equilibrium, the Freundlich, Redlich–Peterson and Sips models show good fits to the experimental data, indicating the heterogeneity of the sorbent surface. The maximum adsorption capacity obtained by the different isotherm models varies between  $104.9 \text{ mg}\cdot\text{g}^{-1}$  and  $133.4 \text{ mg}\cdot\text{g}^{-1}$ . From the study carried out, it can be said that the prepared activated biochar has demonstrated its capacity to adsorb the antibiotic ciprofloxacin in aqueous solutions and is a promising material to be used as an adsorbent for the removal of other drugs and emerging pollutants in aqueous solutions. Therefore, this study can be extended to the adsorption of other compounds of great interest that are dangerous to the environment. On the other hand, to verify the real applicability of activated biochar, studies must be carried out with real effluents, as well as assays, to investigate the regeneration and reuse of the adsorbent material to extend its useful life.

**Supplementary Materials:** The following supporting information can be downloaded at <https://www.mdpi.com/article/10.3390/pr12010199/s1>: Figure S1: CPX speciation as a function of pH and  $\text{pH}_{\text{pzc}}$  of  $\text{K}_2\text{CO}_3$ -activated biochar; Figure S2: Absorption spectra of CPX solutions ( $10 \text{ mg}\cdot\text{L}^{-1}$ ) at acid or basic pH.

**Author Contributions:** Conceptualization, V.F.M., J.F.O., M.I.A., M.L. and A.B.P.-M.; methodology, V.F.M., J.F.O., M.I.A., M.L., A.B.P.-M. and E.F.; software, V.F.M., J.F.O., M.I.A., M.L. and A.B.P.-M.; validation, V.F.M., J.F.O., M.I.A., M.L. and A.B.P.-M.; formal analysis, V.F.M., J.F.O., M.I.A., M.L., A.B.P.-M. and E.F.; investigation, V.F.M., J.F.O., M.I.A., M.L., A.B.P.-M. and E.F.; resources, V.F.M., J.F.O., M.I.A., M.L. and A.B.P.-M.; data curation, V.F.M., J.F.O., M.I.A., M.L., A.B.P.-M. and E.F.; writing—original draft preparation, V.F.M., J.F.O., M.I.A., M.L. and A.B.P.-M.; writing—review and editing, V.F.M., J.F.O., M.I.A., M.L. and A.B.P.-M. All authors have read and agreed to the published version of the manuscript.

**Funding:** This research received no external funding.

**Data Availability Statement:** The data presented in this study are available on request from the corresponding author.

**Acknowledgments:** The authors gratefully acknowledge the support provided by Department of “Enzimología y Biorremediación de Suelos y Residuos Orgánicos” from CEBAS CSIC for allowing the use of a rotary tube furnace.

**Conflicts of Interest:** The authors declare no conflicts of interest.

## References

- Carabineiro, S.A.C.; Thavorn-Amornsri, T.; Pereira, M.F.R.; Serp, P.; Figueiredo, J.L. Comparison between Activated Carbon, Carbon Xerogel and Carbon Nanotubes for the Adsorption of the Antibiotic Ciprofloxacin. *Catal. Today* **2012**, *186*, 29–34. [[CrossRef](#)]
- Lillenberg, M.; Litvin, S.V.; Nei, L.; Roasto, M.; Sepp, K. Enrofloxacin and Ciprofloxacin Uptake by Plants from Soil. *Agron. Res.* **2010**, *8*, 807–814.
- Nguyen, T.T.; Bui, X.T.; Luu, V.P.; Nguyen, P.D.; Guo, W.; Ngo, H.H. Removal of Antibiotics in Sponge Membrane Bioreactors Treating Hospital Wastewater: Comparison between Hollow Fiber and Flat Sheet Membrane Systems. *Bioresour. Technol.* **2017**, *240*, 42–49. [[CrossRef](#)]
- González, J.A.; Bafico, J.G.; Villanueva, M.E.; Giorgieri, S.A.; Copello, G.J. Continuous Flow Adsorption of Ciprofloxacin by Using a Nanostructured Chitin/Graphene Oxide Hybrid Material. *Carbohydr. Polym.* **2018**, *188*, 213–220. [[CrossRef](#)]
- Mondal, S.K.; Saha, A.K.; Sinha, A. Removal of Ciprofloxacin Using Modified Advanced Oxidation Processes: Kinetics, Pathways and Process Optimization. *J. Clean. Prod.* **2018**, *171*, 1203–1214. [[CrossRef](#)]
- Wu, S.; Zhao, X.; Li, Y.; Zhao, C.; Du, Q.; Sun, J.; Wang, Y.; Peng, X.; Xia, Y.; Wang, Z.; et al. Adsorption of Ciprofloxacin onto Biocomposite Fibers of Graphene Oxide/Calcium Alginate. *Chem. Eng. J.* **2013**, *230*, 389–395. [[CrossRef](#)]
- Wang, Y.X.; Ngo, H.H.; Guo, W.S. Preparation of a Specific Bamboo Based Activated Carbon and Its Application for Ciprofloxacin Removal. *Sci. Total Environ.* **2015**, *533*, 32–39. [[CrossRef](#)]
- Carmalin, S.A.; Lima, E.C. Removal of Emerging Contaminants from the Environment by Adsorption. *Ecotoxicol. Environ. Saf.* **2018**, *150*, 1–17. [[CrossRef](#)]
- Malakootian, M.; Faraji, M.; Malakootian, M.; Nozari, M. Ciprofloxacin Removal from Aqueous Media by Adsorption Process: A Systematic Review and Meta-Analysis. *Desalin. Water Treat.* **2021**, *229*, 252–282. [[CrossRef](#)]
- Jiang, W.T.; Chang, P.H.; Wang, Y.S.; Tsai, Y.; Jean, J.S.; Li, Z.; Krukowski, K. Removal of Ciprofloxacin from Water by Birnessite. *J. Hazard. Mater.* **2013**, *250–251*, 362–369. [[CrossRef](#)]
- Beaubien, A.; Jolicoeur, C. The Toxicity of Various Heavy Metals Salts, Alcohols and Surfactants to Microorganism in a Biodegradation Process: A Flow Microcalorimetry Investigation. In *Toxicity Screening Procedure Using Bacterial Systems*; Liu, D., Dutka, B.J., Eds.; Marcel Dekker: New York, NY, USA, 1984; pp. 261–281.
- Ma, J.; Yang, M.; Yu, F.; Zheng, J. Water-Enhanced Removal of Ciprofloxacin from Water by Porous Graphene Hydrogel. *Sci. Rep.* **2015**, *5*, 13578. [[CrossRef](#)] [[PubMed](#)]
- Jaria, G.; Calisto, V.; Esteves, V.I.; Otero, M. Overview of Relevant Economic and Environmental Aspects of Waste-Based Activated Carbons Aimed at Adsorptive Water Treatments. *J. Clean. Prod.* **2022**, *344*, 130984. [[CrossRef](#)]
- Abukari, A.; Abukari Imoro, Z.; Zarouk Imoro, A.; Ballu Duwiejuah, A. Sustainable Use of Biochar in Environmental Management. In *Environmental Health*; IntechOpen: London, UK, 2021.
- Li, F.; Feng, D.; Deng, H.; Yu, H.; Ge, C. Effects of Biochars Prepared from Cassava Dregs on Sorption Behavior of Ciprofloxacin. *Procedia Environ. Sci.* **2016**, *31*, 795–803. [[CrossRef](#)]
- Li, J.; Yu, G.; Pan, L.; Li, C.; You, F.; Xie, S.; Wang, Y.; Ma, J.; Shang, X. Study of Ciprofloxacin Removal by Biochar Obtained from Used Tea Leaves. *J. Environ. Sci.* **2018**, *73*, 20–30. [[CrossRef](#)] [[PubMed](#)]
- Li, R.; Wang, Z.; Guo, J.; Li, Y.; Zhang, H.; Zhu, J.; Xie, X. Enhanced Adsorption of Ciprofloxacin by KOH Modified Biochar Derived from Potato Stems and Leaves. *Water Sci. Technol.* **2018**, *77*, 1127–1136. [[CrossRef](#)]
- Li, R.; Wang, Z.; Zhao, X.; Li, X.; Xie, X. Magnetic Biochar-Based Manganese Oxide Composite for Enhanced Fluoroquinolone Antibiotic Removal from Water. *Environ. Sci. Pollut. Res.* **2018**, *25*, 31136–31148. [[CrossRef](#)]

19. Singh, M.; Ahsan, M.; Pandey, V.; Singh, A.; Mishra, D.; Tiwari, N.; Singh, P.; Karak, T.; Khare, P. Comparative Assessment for Removal of Anionic Dye from Water by Different Waste-Derived Biochar Vis a Vis Reusability of Generated Sludge. *Biochar* **2022**, *4*, 13. [[CrossRef](#)]
20. Mutavdžić Pavlović, D.; Ćurković, L.; Grčić, I.; Šimić, I.; Župan, J. Isotherm, Kinetic, and Thermodynamic Study of Ciprofloxacin Sorption on Sediments. *Environ. Sci. Pollut. Res.* **2017**, *24*, 10091–10106. [[CrossRef](#)]
21. Ambaye, T.G.; Vaccari, M.; van Hullebusch, E.D.; Amrane, A.; Rtimi, S. Mechanisms and Adsorption Capacities of Biochar for the Removal of Organic and Inorganic Pollutants from Industrial Wastewater. *Int. J. Environ. Sci. Technol.* **2021**, *18*, 3273–3294. [[CrossRef](#)]
22. Tan, X.; Liu, S.; Liu, Y.; Gu, Y.; Zeng, G.; Hu, X.; Wang, X.; Liu, S.; Jiang, L. Biochar as Potential Sustainable Precursors for Activated Carbon Production: Multiple Applications in Environmental Protection and Energy Storage. *Bioresour. Technol.* **2017**, *227*, 359–372. [[CrossRef](#)]
23. Xiong, Z.; Huanhuan, Z.; Jing, W.; Wei, C.; Yingquan, C.; Gao, X.; Haiping, Y.; Hanping, C. Physicochemical and Adsorption Properties of Biochar from Biomass-Based Pyrolytic Polygeneration: Effects of Biomass Species and Temperature. *Biochar* **2021**, *3*, 657–670. [[CrossRef](#)]
24. Zhang, B.; Han, X.; Gu, P.; Fang, S.; Bai, J. Response Surface Methodology Approach for Optimization of Ciprofloxacin Adsorption Using Activated Carbon Derived from the Residue of Desilicated Rice Husk. *J. Mol. Liq.* **2017**, *238*, 316–325. [[CrossRef](#)]
25. Zeng, Z.W.; Tian, S.R.; Liu, Y.G.; Tan, X.F.; Zeng, G.M.; Jiang, L.H.; Yin, Z.H.; Liu, N.; Liu, S.B.; Li, J. Comparative Study of Rice Husk Biochars for Aqueous Antibiotics Removal. *J. Chem. Technol. Biotechnol.* **2018**, *93*, 1075–1084. [[CrossRef](#)]
26. Huang, W.; Chen, J.; Zhang, J. Removal of Ciprofloxacin from Aqueous Solution by Rabbit Manure Biochar. *Environ. Technol.* **2020**, *41*, 1380–1390. [[CrossRef](#)] [[PubMed](#)]
27. Ashiq, A.; Sarkar, B.; Adassooriya, N.; Walpita, J.; Rajapaksha, A.U.; Ok, Y.S.; Vithanage, M. Sorption Process of Municipal Solid Waste Biochar-Montmorillonite Composite for Ciprofloxacin Removal in Aqueous Media. *Chemosphere* **2019**, *236*, 124384. [[CrossRef](#)]
28. Li, J.; Yu, G.; Pan, L.; Li, C.; You, F.; Wang, Y. Ciprofloxacin Adsorption by Biochar Derived from Co-Pyrolysis of Sewage Sludge and Bamboo Waste. *Environ. Sci. Pollut. Res.* **2020**, *27*, 22806–22817. [[CrossRef](#)]
29. Patel, M.; Kumar, R.; Pittman, C.U.; Mohan, D. Ciprofloxacin and Acetaminophen Sorption onto Banana Peel Biochars: Environmental and Process Parameter Influences. *Environ. Res.* **2021**, *201*, 111218. [[CrossRef](#)]
30. Sayin, F.; Akar, S.T.; Akar, T. From Green Biowaste to Water Treatment Applications: Utilization of Modified New Biochar for the Efficient Removal of Ciprofloxacin. *Sustain. Chem. Pharm.* **2021**, *24*, 100522. [[CrossRef](#)]
31. Özer, Ç.; İmamoğlu, M. Removal of Ciprofloxacin from Aqueous Solutions by Pumpkin Peel Biochar Prepared Using Phosphoric Acid. *Biomass Convers. Biorefinery* **2022**, *1*, 3. [[CrossRef](#)]
32. Kunze, W.; Manger, H.-J.; Pratt, S. *Technology Brewing and Malting*; VLB: Berlin, Germany, 2014; ISBN 9783921690772.
33. Mussatto, S.I. Biotechnological Potential of Brewing Industry By-Products. In *Biotechnology for Agro-Industrial Residues Utilisation: Utilisation of Agro-Residues*; Springer: Dordrecht, The Netherlands, 2009; pp. 313–326, ISBN 9781402099410.
34. de Araújo, T.P.; Quesada, H.B.; Bergamasco, R.; Vareschini, D.T.; de Barros, M.A.S.D. Activated Hydrochar Produced from Brewer's Spent Grain and Its Application in the Removal of Acetaminophen. *Bioresour. Technol.* **2020**, *310*, 123399. [[CrossRef](#)]
35. Sousa, A.F.C.; Gil, M.V.; Calisto, V. Upcycling Spent Brewery Grains through the Production of Carbon Adsorbents—Application to the Removal of Carbamazepine from Water. *Environ. Sci. Pollut. Res.* **2020**, *27*, 36463–36475. [[CrossRef](#)] [[PubMed](#)]
36. Sousa, É.M.L.; Otero, M.; Rocha, L.S.; Gil, M.V.; Ferreira, P.; Esteves, V.I.; Calisto, V. Multivariable Optimization of Activated Carbon Production from Microwave Pyrolysis of Brewery Wastes—Application in the Removal of Antibiotics from Water. *J. Hazard. Mater.* **2022**, *431*, 128556. [[CrossRef](#)]
37. Sevilla, M.; Fuertes, A.B. A Green Approach to High-Performance Supercapacitor Electrodes: The Chemical Activation of Hydrochar with Potassium Bicarbonate. *ChemSusChem* **2016**, *9*, 1880–1888. [[CrossRef](#)] [[PubMed](#)]
38. Ahmad, M.; Rajapaksha, A.U.; Lim, J.E.; Zhang, M.; Bolan, N.; Mohan, D.; Vithanage, M.; Lee, S.S.; Ok, Y.S. Biochar as a Sorbent for Contaminant Management in Soil and Water: A Review. *Chemosphere* **2014**, *99*, 19–33. [[CrossRef](#)] [[PubMed](#)]
39. Yang, Y.; Phuong Nguyen, T.M.; Van, H.T.; Nguyen, Q.T.; Nguyen, T.H.; Lien Nguyen, T.B.; Hoang, L.P.; Van Thanh, D.; Nguyen, T.V.; Nguyen, V.Q.; et al. ZnO Nanoparticles Loaded Rice Husk Biochar as an Effective Adsorbent for Removing Reactive Red 24 from Aqueous Solution. *Mater. Sci. Semicond. Process.* **2022**, *150*, 106960. [[CrossRef](#)]
40. Sánchez-García, M.; Cayuela, M.L.; Rasse, D.P.; Sánchez-Monedero, M.A. Biochars from Mediterranean Agroindustry Residues: Physicochemical Properties Relevant for C Sequestration and Soil Water Retention. *ACS Sustain. Chem. Eng.* **2019**, *7*, 4724–4733. [[CrossRef](#)]
41. Iriarte-Velasco, U.; Ayastuy, J.L.; Zudaire, L.; Sierra, I. An Insight into the Reactions Occurring during the Chemical Activation of Bone Char. *Chem. Eng. J.* **2014**, *251*, 217–227. [[CrossRef](#)]
42. Cha, J.S.; Park, S.H.; Jung, S.C.; Ryu, C.; Jeon, J.K.; Shin, M.C.; Park, Y.K. Production and Utilization of Biochar: A Review. *J. Ind. Eng. Chem.* **2016**, *40*, 1–15. [[CrossRef](#)]
43. Zhu, L.; Zhao, N.; Tong, L.; Lv, Y. Structural and Adsorption Characteristics of Potassium Carbonate Activated Biochar. *RSC Adv.* **2018**, *8*, 21012–21019. [[CrossRef](#)]
44. Rivera-Utrilla, J.; Bautista-Toledo, I.; Ferro-García, M.A.; Moreno-Castilla, C. Activated Carbon Surface Modifications by Adsorption of Bacteria and Their Effect on Aqueous Lead Adsorption. *J. Chem. Technol. Biotechnol.* **2001**, *76*, 1209–1215. [[CrossRef](#)]

45. Fiol, N.; Villaescusa, I. Determination of Sorbent Point Zero Charge: Usefulness in Sorption Studies. *Environ. Chem. Lett.* **2009**, *7*, 79–84. [[CrossRef](#)]
46. Movasaghi, Z.; Yan, B.; Niu, C. Adsorption of Ciprofloxacin from Water by Pretreated Oat Hulls: Equilibrium, Kinetic, and Thermodynamic Studies. *Ind. Crops Prod.* **2019**, *127*, 237–250. [[CrossRef](#)]
47. Miller, J.N.; Miller, J.C. *Statistics and Chemometrics for Analytical Chemistry*, 7th ed.; Pearson Education Limited: London, UK, 2018; ISBN 9780273730422.
48. Mocak, J.; Bond, A.M.; Mitchell, S.; Scollary, G. International Union of Pure and Applied Chemistry. Analytical Chemistry Division Commission on Electroanalytical Chemistry A Statistical Overview of Standard (IUPAC and ACS) and New Procedures for Determining the Limits of Detection and Quantification: Ap. *Pure Appl. Chem* **1997**, *69*, 297–328. [[CrossRef](#)]
49. Barkakati, P.; Begum, A.; Das, M.L.; Rao, P.G. Adsorptive Separation of Ginsenoside from Aqueous Solution by Polymeric Resins: Equilibrium, Kinetic and Thermodynamic Studies. *Chem. Eng. J.* **2010**, *161*, 34–45. [[CrossRef](#)]
50. Majd, M.M.; Kordzadeh-Kermani, V.; Ghalandari, V.; Askari, A.; Sillanpää, M. Adsorption Isotherm Models: A Comprehensive and Systematic Review (2010–2020). *Sci. Total Environ.* **2022**, *812*, 151334. [[CrossRef](#)] [[PubMed](#)]
51. Hadjiivanov, K. Identification and Characterization of Surface Hydroxyl Groups by Infrared Spectroscopy. In *Advances in Catalysis*; Elsevier: Amsterdam, The Netherlands, 2014; pp. 99–318.
52. Shabanian, M.; Hajibeygi, M.; Raeisi, A. FTIR Characterization of Layered Double Hydroxides and Modified Layered Double Hydroxides. In *Layered Double Hydroxide Polymer Nanocomposites*; Elsevier: Amsterdam, The Netherlands, 2020; pp. 77–101.
53. Meseguer, V.F.; Ortuño, J.F.; Aguilar, M.I.; Pinzón-Bedoya, M.L.; Lloréns, M.; Sáez, J.; Pérez-Marín, A.B. Biosorption of Cadmium (II) from Aqueous Solutions by Natural and Modified Non-Living Leaves of *Posidonia Oceanica*. *Environ. Sci. Pollut. Res.* **2016**, *23*, 24032–24046. [[CrossRef](#)] [[PubMed](#)]
54. Zhao, J.; Liang, G.; Zhang, X.; Cai, X.; Li, R.; Xie, X.; Wang, Z. Coating Magnetic Biochar with Humic Acid for High Efficient Removal of Fluoroquinolone Antibiotics in Water. *Sci. Total Environ.* **2019**, *688*, 1205–1215. [[CrossRef](#)]
55. Ma, Y.; Li, M.; Li, P.; Yang, L.; Wu, L.; Gao, F.; Qi, X.; Zhang, Z. Hydrothermal Synthesis of Magnetic Sludge Biochar for Tetracycline and Ciprofloxacin Adsorptive Removal. *Bioresour. Technol.* **2021**, *319*, 124199. [[CrossRef](#)]
56. Egbedina, A.O.; Adebowale, K.O.; Olu-Owolabi, B.I.; Unuabonah, E.I.; Adesina, M.O. Green Synthesis of ZnO Coated Hybrid Biochar for the Synchronous Removal of Ciprofloxacin and Tetracycline in Wastewater. *RSC Adv.* **2021**, *11*, 18483–18492. [[CrossRef](#)]
57. Zhou, Y.; Cao, S.; Xi, C.; Li, X.; Zhang, L.; Wang, G.; Chen, Z. A Novel Fe<sub>3</sub>O<sub>4</sub>/Graphene Oxide/Citrus Peel-Derived Bio-Char Based Nanocomposite with Enhanced Adsorption Affinity and Sensitivity of Ciprofloxacin and Sparfloxacin. *Bioresour. Technol.* **2019**, *292*, 121951. [[CrossRef](#)]
58. Hu, Y.; Zhu, Y.; Zhang, Y.; Lin, T.; Zeng, G.; Zhang, S.; Wang, Y.; He, W.; Zhang, M.; Long, H. An Efficient Adsorbent: Simultaneous Activated and Magnetic ZnO Doped Biochar Derived from Camphor Leaves for Ciprofloxacin Adsorption. *Bioresour. Technol.* **2019**, *288*, 121511. [[CrossRef](#)] [[PubMed](#)]

**Disclaimer/Publisher’s Note:** The statements, opinions and data contained in all publications are solely those of the individual author(s) and contributor(s) and not of MDPI and/or the editor(s). MDPI and/or the editor(s) disclaim responsibility for any injury to people or property resulting from any ideas, methods, instructions or products referred to in the content.